

Valley-Layer Coupling: A New Design Principle for Valleytronics

Zhi-Ming Yu^{1,2}, Shan Guan,^{3,2} Xian-Lei Sheng,^{4,2,*} Weibo Gao,^{5,6,†} and Shengyuan A. Yang^{2,‡}

¹Key Lab of Advanced Optoelectronic Quantum Architecture and Measurement (MOE),
Beijing Key Lab of Nanophotonics & Ultrafine Optoelectronic Systems,
and School of Physics, Beijing Institute of Technology, Beijing 100081, China

²Research Laboratory for Quantum Materials, Singapore University of Technology and Design, Singapore 487372, Singapore

³State Key Laboratory of Superlattices and Microstructures, Institute of Semiconductors,
Chinese Academy of Sciences, Beijing 100083, China

⁴Department of Physics, Key Laboratory of Micro-nano Measurement-Manipulation and Physics (Ministry of Education),
Beihang University, Beijing 100191, China

⁵Division of Physics and Applied Physics, School of Physical and Mathematical Sciences,
Nanyang Technological University, Singapore 637371, Singapore

⁶The Photonics Institute and Centre for Disruptive Photonic Technologies,
Nanyang Technological University, Singapore 637371, Singapore



(Received 15 April 2019; published 23 January 2020)

The current valleytronics research is based on the paradigm of time-reversal-connected valleys in two-dimensional (2D) hexagonal materials, which forbids the fully electric generation of valley polarization by a gate field. Here, we go beyond the existing paradigm to explore 2D systems with a novel valley-layer coupling (VLC) mechanism, where the electronic states in the emergent valleys have a valley-contrasted layer polarization. The VLC enables a direct coupling between a valley and a gate electric field. We analyze the symmetry requirements for a system to host VLC, demonstrate our idea via first-principles calculations and model analysis of a concrete 2D material example, and show that an electric, continuous, wide-range, and switchable control of valley polarization can be achieved by VLC. Furthermore, we find that systems with VLC can exhibit other interesting physics, such as valley-contrasting linear dichroism and optical selection of the valley and the electric polarization of interlayer excitons. Our finding opens a new direction for valleytronics and 2D materials research.

DOI: [10.1103/PhysRevLett.124.037701](https://doi.org/10.1103/PhysRevLett.124.037701)

Introduction.—The electronic conduction and/or valence band in materials may feature multiple energy extremal points in the momentum space, which endows the low-energy electrons with an additional valley degree of freedom (d.o.f.). Analogous to spin, this valley freedom can be utilized to encode and process information, giving rise to the concept of valleytronics [1–7]. In the past decade, with the discovery of two-dimensional (2D) valleytronic materials in graphene and transitional metal dichalcogenides (TMD), the field of valleytronics has undergone rapid development and attracted broad interest at both fundamental and applied levels [1,8–29].

The current valleytronics research has been mainly established in the paradigm of time-reversal (\mathcal{T}) connected valleys in 2D hexagonal lattices [10,11]. (Valley physics in 2D rectangular-lattice SnS was studied in Refs. [30–32].) There, the two valleys K and K' are differentiated by geometric properties like Berry curvature and orbital magnetic moment which are odd functions under \mathcal{T} [33,34]. To generate valley polarization, which is the prerequisite for valleytronics, one has to break the \mathcal{T} symmetry, either by an applied magnetic field [7,35–40], or by a dynamical process, e.g., optical pumping with circularly polarized light [41–45],

spin injection [46], or valley Hall effect [47–49]. However, for device applications, static means are preferred than dynamic means, and fully electric control is preferred over magnetic or optical control. Particularly, static control by gate electric field is most desirable, owing to its advantages in compactness, power efficiency, and compatibility with existing semiconductor technology. Evidently, the gate field cannot couple to the valley, because it does not break \mathcal{T} . This poses an outstanding challenge for the field of valleytronics, and, to solve this problem, one must go beyond the existing valleytronics paradigm.

Here, we present a disruptively new design principle for valleytronics to tackle this challenge. The idea is to explore systems in which the valleys are connected by a crystalline symmetry instead of \mathcal{T} , thereby circumventing the fundamental restriction posed by symmetry. We impose constraints on the crystalline symmetry, such that the system can admit a special coupling between valley and a spatial d.o.f., which is termed as the valley-layer coupling (VLC). VLC enables a direct interaction between the valley and the gate electric field, as schematically illustrated in Fig. 1. We demonstrate our ideas via first-principles calculations and model analysis of a concrete 2D material example.

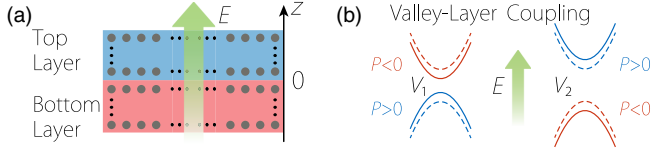


FIG. 1. (a) A 2D material system viewed as consisting of two layers. Each layer may consist of a few atomic layers. (b) With valley-contrasting layer polarization (P), an applied gate electrical field can generate valley polarization. The solid (dashed) curves denote the bands in the presence (absence) of the electric field. $P > 0$ ($P < 0$) means the state is mainly localized on the top (bottom) layer.

Besides the gate-field control of valley polarization, we show that systems with VLC exhibit additional interesting physics, such as valley-contrasting linear dichroism and optical manipulation of interlayer excitons with selected valley and electric polarization. Since the interlayer exciton has a dipole along the sample growth direction, it leads to the possibility of electric control and trapping of excitons, which can further facilitate the realization of exciton transistors or dipolar BEC [50,51]. Our work thus not only tackles an outstanding challenge, it also opens a significant new arena for valleytronics research.

Theory of valley-layer coupling.—We consider a 2D material system. The system is extended in the x - y plane, and has a finite thickness along z , which is the direction for the gate field. It can be viewed as consisting of two *layers*: the top layer with $z > 0$ and the bottom layer with $z < 0$, where $z = 0$ is set to be the midpoint of the system along z [see Fig. 1(a)]. Notice that each such layer may contain multiple atomic layers.

In order to discuss VLC, we first define the layer polarization. For a Bloch band eigenstate $\psi_{nk}(\mathbf{r})$, we define its layer polarization $P_n(\mathbf{k})$ as

$$P_n(\mathbf{k}) = \int_{z>0} |\psi_{nk}|^2 d\mathbf{r} - \int_{z<0} |\psi_{nk}|^2 d\mathbf{r}, \quad (1)$$

where n is the band index, $\mathbf{k} = (k_x, k_y)$ is the wave vector in the 2D Brillouin zone (BZ), and the position vector \mathbf{r} has also a z component due to the finite thickness. $P_n(\mathbf{k})$ reflects the polarization of ψ_{nk} between the two layers: $P > 0$ ($P < 0$) means the state has more weight distributed in the top (bottom) layer. This quantity gives us a simple way to infer the behavior of the bands under a gate field. Since the gate field produces a layer-dependent electrostatic potential, states with opposite P are expected to acquire opposite energy shifts.

The concept of VLC can now be intuitively understood as the coupling between the valley d.o.f. and the layer polarization. Analogous to the valley-spin coupling in TMD materials [5], VLC requires the valleys to exhibit valley-contrasting layer polarizations. If realized, it will

naturally achieve the electric control of valleys using gate field, as illustrated in Fig. 1(b).

Next, we analyze the symmetry requirements for a system to host VLC. We consider nonmagnetic systems with a binary valley d.o.f., which means that \mathcal{T} is preserved and there are two inequivalent valleys in the BZ, denoted as V_1 and V_2 . To achieve valley polarization via gate field, the two valleys must *not* be connected by \mathcal{T} . This requires that each valley must be located at a time-reversal-invariant momentum (TRIM) point. Moreover, the two valleys must be connected by a certain crystalline symmetry operation \mathcal{O} to enforce their degeneracy in energy, namely,

$$\mathcal{O}: V_1 \rightleftharpoons V_2. \quad (2)$$

Then, to enable VLC, the following considerations should be satisfied.

(i) The two valleys must have *finite* and *opposite* layer polarizations. This indicates that \mathcal{O} must satisfy the following relation:

$$\mathcal{O}P(V_1)\mathcal{O}^{-1} = -P(V_2). \quad (3)$$

Here, we drop the band index in P , which is understood to be either the lowest conduction band or the highest valence band. This requirement also implies that \mathcal{O} must be broken by the applied gate field.

(ii) To have a finite P at V_1 and V_2 , certain crystalline symmetries must be broken. These include the horizontal mirror reflection \mathcal{M}_z and the inversion \mathcal{I} . Because under their transformations

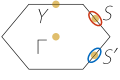

$$\mathcal{M}_z P(V_i) \mathcal{M}_z^{-1} = -P(V_i), \quad \mathcal{I} P(V_i) \mathcal{I}^{-1} = -P(V_i), \quad (4)$$

where $i \in \{1, 2\}$ (we have used the fact that V_1 and V_2 are at TRIM points and hence invariant under these operations), the polarization will be suppressed at the valley if either \mathcal{M}_z or \mathcal{I} is preserved.

Based on the above considerations, one can go through the 80 layer groups (LGs) for 2D materials to screen out the ones that allow the existence of VLC. The results are listed in Table I. One can see that the candidates belong to two 2D Bravais lattices: the centered rectangular lattice (LG 10 and 22) and the square lattice (LG 50, 59, and 60). For LG 10 and 22, the two valleys should appear at TRIM points S and S' , and they are connected by a twofold rotation with an in-plane axis. For LG 50, 59, and 60, the two valleys should sit at X and X' , and they are connected by a roto-reflection \mathcal{S}_{4z} (for LG 59 and 60, a twofold rotation along $[110]$ also connects them). For a 2D material falling into one of these groups, as long as its conduction or valence band edge occurs at the requested TRIM points, it will generally host VLC and permit the gate control of the valley d.o.f.

Application to a concrete example.—Having established the theory of VLC, below, we illustrate our key idea with a

TABLE I. Layer groups allowing for VLC. In the second column, the red and blue circles denote the two valleys V_1 and V_2 . The last column shows the corresponding space group [52].

Lattice	BZ	Valleys (V_1, V_2)	Layer group	Symmetry \mathcal{O}	Space group
Centered rectangular		(S, S')	10 ($c211$)	$\{C_{2x} 000\}$	5
			22 ($c222$)	$\{C_{2x} 000\}, \{C_{2y} 000\}$	21
			50 ($p\bar{4}$)	$\{S_{4z} 000\}$	81
Square		(X, X')	59 ($P\bar{4}m2$)	$\{S_{4z} 000\}, \{C_{2,110} 000\}$	115
			60 ($p4b2$)	$\{S_{4z} 000\}, \{C_{2,110} \frac{1}{2}\frac{1}{2}0\}$	117

concrete example. The symmetry conditions obtained above (Table I) offer useful guidance in searching for suitable material systems. Here, we consider the monolayer TiSiCO (ML-TSCO). As illustrated in Fig. 2, it has similar structure as ML-HfGeTe [53] and ML-ZrSiO studied before [54]. It possesses five square-lattice atomic layers vertically stacked in the sequence of O-Ti-Si/C-Ti-O, with LG No. 59 ($P\bar{4}m2$), which is one candidate in Table I. Via first-principles calculations, we confirm that the monolayer is dynamically stable [see Fig. 2(d)] and also enjoys good thermal stability up to 800 K [55]. The optimized lattice constant is $a = b = 2.817 \text{ \AA}$. As we shall see, the low-energy states in ML-TSCO are mainly distributed in the two Ti layers. It is worth noting that the two Ti layers have a separation about 4.1 \AA , which is even comparable to the typical interlayer separation for van der Waals stacked heterostructures.

According to Table I, a material with LG 59 can host VLC if it has valleys located at X and X' points. This is indeed the case for ML-TSCO. Figure 3(a) shows the calculated electronic band structure. Here, the spin-orbit coupling (SOC) is not included because of its negligible strength for this material. One clearly observes that a pair of valleys for both conduction and valence bands occur at X and X' . The two valleys are connected by S_{4z} and $C_{2,[110]}$, rather than \mathcal{T} . Hence, according to our previous analysis, they must have finite and opposite layer polarizations. By analyzing the spatial distribution of the states [see Figs. 3(a)–3(b)], one finds the following features. (i) The band edge states are mainly distributed in the two Ti layers. (ii) The conduction band at X valley is mainly distributed in the bottom layer,

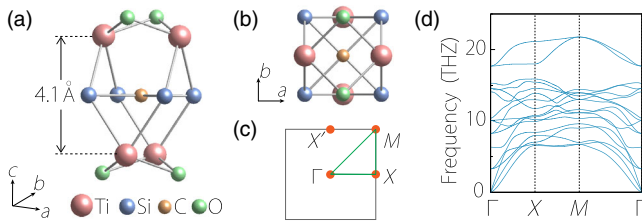
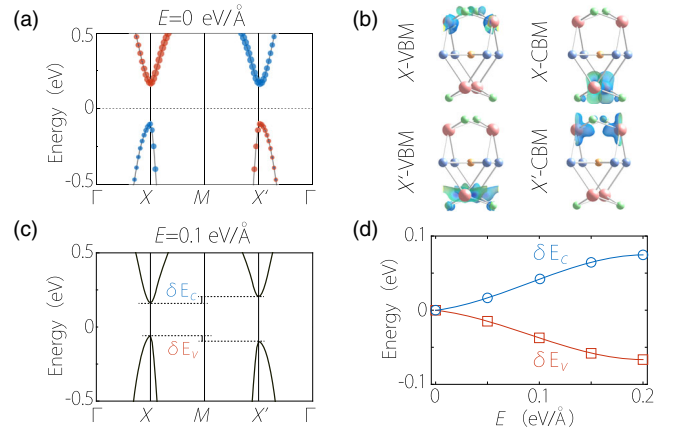


FIG. 2. (a) Side view and (b) top view of the crystal structure for monolayer TiSiCO. (c) The corresponding BZ. (d) Phonon spectrum for ML-TSCO.

whereas for the X' valley it is mainly in the top layer. (iii) The layer distribution pattern for the valence bands is reversed. The physical picture corresponds to the schematic illustration in Fig. 1(b). Thus, the first-principles calculation confirms the existence of VLC, consistent with our theory.

To demonstrate that VLC indeed enables the gate control of valleys, we explicitly calculate the band structure under a vertical electric field. As shown in Fig. 3(c), for the conduction band, the gate field pulls down the X valley and pushes up the X' valley, successfully generating a valley polarization for the electron carriers when the system is n doped. For the valence band, the valley shifts are opposite, due to the reversed layer polarization, so valley polarization can also be generated for holes when the system is p doped. Our calculation shows that for ML-TSCO, a gate field of 0.1 eV/\AA (achievable with current experimental technique [62]) can induce a valley energy splitting of 37 and 42 meV for valence and conduction bands, respectively [see Fig. 3(d)]. Such energy scale is larger than the thermal energy at room temperature,


 FIG. 3. (a) Electronic band structure for ML-TSCO. The size of the red (blue) dots in (a) is proportional to the weight of projection onto atomic orbitals in the bottom (top) Ti atoms. (b) Charge density distribution plotted for VBM and CBM states at the two valleys. (c) shows the band structure under a gate field of $E = 0.1 \text{ eV/\AA}$. (d) Valley splitting for VBM (δE_v) and CBM (δE_c) [indicated in (c)] versus the applied gate field.

suggesting its potential for room-temperature device operations.

Effective model for VLC.—To better understand the physics of VLC, we develop an effective model based on the above result for ML-TSCO. Here, the low-energy physics occur at X and X' , both having the little group of C_{2v} . At X (X') point, the CBM ψ_c and the VBM ψ_v correspond to the 1D representations B_2 and A_1 (B_1 and A_1) for the C_{2v} group. Using them as basis states, the kp effective model expanded up to linear order reads [55]

$$\mathcal{H}_0 = \Delta\sigma_z + v(k_x + k_y)\sigma_y - v(k_x - k_y)\tau_z\sigma_y, \quad (5)$$

where the wave vector \mathbf{k} is measured from each valley center, Δ represents half the band gap, $\tau_z = \pm 1$ denotes the X/X' valley, and σ s are Pauli matrices acting on the basis of one valley $\Psi^V = (\psi_c^V, \psi_v^V)^T$ with $V \in \{X, X'\}$. Since ψ_c and ψ_v are, respectively, polarized in the top and bottom layers, σ can also be regarded as acting on the layer index space, and, in particular, the layer polarization for a state ψ is given by $P_\psi = \langle \psi | \sigma_z | \psi \rangle$. The last term in (5) involving $\tau_z\sigma_y$ clearly indicates a coupling between valley and layer d.o.f. Since the two valley basis Ψ^X and $\Psi^{X'}$ are connected by \mathcal{S}_{4z} , which reverses P , the effect of gate field is captured by

$$\mathcal{H}_E = \Delta_E \tau_z \sigma_z, \quad (6)$$

where the effective strength Δ_E may be taken as linear in the E field, i.e., $\Delta_E = \alpha E$, in the simplest approximation. It follows that the applied E field shifts the band edges at the two valleys in opposite ways, and the local gaps at the two valleys become $2(\Delta \pm \Delta_E)$. The model parameters can be obtained by fitting the DFT results that $\Delta = 0.133$ eV, $v = 0.59$ eV Å and $\alpha \approx -0.2$ Å.

Valley linear dichroism and interlayer exciton.—Since the two valleys are characterized by C_{2v} symmetry and are connected by \mathcal{S}_{4z} , they should exhibit valley-contrasting linear dichroism in the optical interband absorption. This can be readily verified by using the effective model in Eq. (5). The coupling strength with optical fields linearly polarized in the i th direction is given by

$$M_i(\mathbf{k}) = m_e \langle u_c(\mathbf{k}) | \frac{\partial \mathcal{H}}{\partial k_i} | u_v(\mathbf{k}) \rangle, \quad (7)$$

where m_e is the free electron mass, and $u_{c(v)}$ the periodic part of the Bloch state of conduction (valence) band. With the model in Eq. (5), we find that, for the X valley,

$$|M_x^X(\mathbf{k})|^2 = O(k^2), \quad |M_y^X(\mathbf{k})|^2 = \frac{4v^2 m_e^2 \Delta^2}{4v^2 k_y^2 + \Delta^2}. \quad (8)$$

Similarly, for the X' valley, we have

$$M_{x/y}^{X'}(k_x, k_y) = M_{y/x}^X(-k_y, k_x). \quad (9)$$

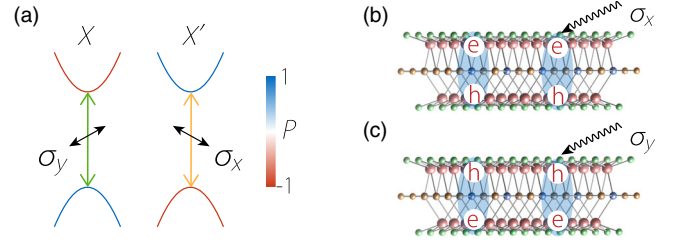


FIG. 4. (a) Valley optical transition selection rules. (b) X' and (c) X valley-polarized interlayer excitons with opposite electric polarization can be selectively excited by σ_x and σ_y linear polarized optical fields, respectively. This optical selection of the electric dipole of interlayer excitons is a unique phenomenon only associated with VLC.

Close to the valley center, the interband transitions are coupled exclusively with x -linearly (y -linearly) polarized light for the X' (X) valley, consistent with our symmetry argument, as shown in Fig. 4(a). This means that we can selectively excite carriers in one valley by controlling the polarization of light. Applying a gate electric field will not affect the linear dichroism, but can further split the band edge transition frequency by $4\Delta_E$ for the two valleys. We note that valley-selective linear dichroism was also observed for 2D SnS [30–32], but the valley physics is distinct, as VLC is forbidden there due to the existence of a horizontal glide mirror.

Here, due to the layer polarization of the valley states, for a particular valley, the optically excited electrons and holes are located at different layers. The interaction between the electrons and holes leads to the formation of excitons. Interestingly, the excitons here are interlayer excitons with valley-contrasting layer polarization. As illustrated in Fig. 4(b), the x -polarized light with the band edge excitonic transition frequency will selectively generate excitons in the X' valley, with holes in the top layer and electrons in the bottom layer. The situation is reversed for the y -polarized light [see Fig. 4(c)]. Note that these interlayer excitons naturally carry a charge polarization along z , so they can be electrically manipulated [63–67] and the effect of linear dichroism can also be probed by voltage measurement across the thickness. Remarkably, the interlayer exciton here is distinct from those demonstrated in heterogeneous TMD bilayers [10,65–69]: the polarization of the excitons there is fixed by the type-II band alignment of the structure, whereas the polarization here can be selected by controlling the light polarization.

Discussion.—In this work, we have proposed a new design principle to achieve static control of valley polarization by a gate electric field. The essence is to switch the focus from conventional T -connected valleys to crystal-symmetry-connected valleys with VLC.

We point out that such electrically generated valley polarization may also permit a purely electric detection. Note that each valley in LG 59 and 60 only has twofold

rotational symmetry, indicating that the dispersion in the valley must be anisotropic. For example, in ML-TSCO, for the X valley, the effective mass of valence band along x is $m_x^* \approx 0.84m_e$, whereas $m_y^* \approx 0.16m_e$, differing by ~ 5 times. Because of \mathcal{S}_{4z} , the anisotropy at the X' valley is rotated by $\pi/2$, so that in the absence of valley polarization, the transport properties are still isotropic. The valley polarization breaks the \mathcal{S}_{4z} symmetry, making the transport anisotropic. For example, ML-TSCO with X valley polarization should have a larger resistance along x than y . By measuring the anisotropic resistance, one can readily detect the valley polarization. Thus, both valley information write in and read off can be achieved by purely electric means, which is a great advantage of our scheme.

The optical properties revealed here would endow the system with additional possibilities. For example, the valley polarization can also be optically detected by the difference in the optical absorbances for x and y polarized lights. In addition, the interlayer excitons, which can be selectively created here by linearly polarized light, are expected to have longer lifetime due to the spatial separation between electron and hole, which is desirable for exciton valleytronics [10,70,71] and for achieving more exotic phases such as exciton condensation [72,73].

The authors thank D. L. Deng for helpful discussions. This work is supported by the Singapore MOE AcRF Tier 2 (MOE2017-T2-2-108), the Singapore National Research Foundation (NRF-NRFF2015-03) and its Competitive Research Program (CRP Award NRF-CRP21-2018-0007), and the NSFC (Grants No. 11834014, No. 11504013, and No. 11904359).

Z.-M. Y. and S. G. contributed equally to this work.

*xlsheng@buaa.edu.cn

†wbgao@ntu.edu.sg

‡shengyuan_yang@sutd.edu.sg

- [1] A. Rycerz, J. Tworzydło, and C. Beenakker, *Nat. Phys.* **3**, 172 (2007).
- [2] O. Gunawan, Y. P. Shkolnikov, K. Vakili, T. Gokmen, E. P. De Poortere, and M. Shayegan, *Phys. Rev. Lett.* **97**, 186404 (2006).
- [3] D. Xiao, W. Yao, and Q. Niu, *Phys. Rev. Lett.* **99**, 236809 (2007).
- [4] W. Yao, D. Xiao, and Q. Niu, *Phys. Rev. B* **77**, 235406 (2008).
- [5] D. Xiao, G.-B. Liu, W. Feng, X. Xu, and W. Yao, *Phys. Rev. Lett.* **108**, 196802 (2012).
- [6] Z. Zhu, A. Collaudin, B. Fauqué, W. Kang, and K. Behnia, *Nat. Phys.* **8**, 89 (2012).
- [7] T. Cai, S. A. Yang, X. Li, F. Zhang, J. Shi, W. Yao, and Q. Niu, *Phys. Rev. B* **88**, 115140 (2013).
- [8] X. Xu, W. Yao, D. Xiao, and T. F. Heinz, *Nat. Phys.* **10**, 343 (2014).
- [9] G. B. Liu, D. Xiao, Y. Yao, X. Xu, and W. Yao, *Chem. Soc. Rev.* **44**, 2643 (2015).
- [10] J. R. Schaibley, H. Yu, G. Clark, P. Rivera, J. S. Ross, K. L. Seyler, W. Yao, and X. Xu, *Nat. Rev. Mater.* **1**, 16055 (2016).
- [11] S. A. Vitale, D. Nezich, J. O. Varghese, P. Kim, N. Gedik, P. Jarillo-Herrero, D. Xiao, and M. Rothschild, *Small* **14**, e1801483 (2018).
- [12] D. Gunlycke and C. T. White, *Phys. Rev. Lett.* **106**, 136806 (2011).
- [13] H. Pan, X. Li, F. Zhang, and S. A. Yang, *Phys. Rev. B* **92**, 041404(R) (2015).
- [14] H. Pan, X. Li, H. Jiang, Y. Yao, and S. A. Yang, *Phys. Rev. B* **91**, 045404 (2015).
- [15] Y. Jiang, T. Low, K. Chang, M. I. Katsnelson, and F. Guinea, *Phys. Rev. Lett.* **110**, 046601 (2013).
- [16] M. M. Grujić, M. Z. Tadić, and F. M. Peeters, *Phys. Rev. Lett.* **113**, 046601 (2014).
- [17] L. Ju, Z. Shi, N. Nair, Y. Lv, C. Jin, J. Velasco, Jr., C. Ojeda-Aristizabal, H. A. Bechtel, M. C. Martin, A. Zettl *et al.*, *Nature (London)* **520**, 650 (2015).
- [18] M. Sui, G. Chen, L. Ma, W.-Y. Shan, D. Tian, K. Watanabe, T. Taniguchi, X. Jin, W. Yao, D. Xiao *et al.*, *Nat. Phys.* **11**, 1027 (2015).
- [19] W. Y. Tong, S. J. Gong, X. Wan, and C. G. Duan, *Nat. Commun.* **7**, 13612 (2016).
- [20] V. H. Nguyen, S. Dechamps, P. Dollfus, and J.-C. Charlier, *Phys. Rev. Lett.* **117**, 247702 (2016).
- [21] A. R. Akhmerov, J. H. Bardarson, A. Rycerz, and C. W. J. Beenakker, *Phys. Rev. B* **77**, 205416 (2008).
- [22] A. Cresti, G. Grosso, and G. P. Parravicini, *Phys. Rev. B* **77**, 233402 (2008).
- [23] P. San-Jose, E. Prada, E. McCann, and H. Schomerus, *Phys. Rev. Lett.* **102**, 247204 (2009).
- [24] Z. Qiao, J. Jung, Q. Niu, and A. H. MacDonald, *Nano Lett.* **11**, 3453 (2011).
- [25] Z. Qiao, J. Jung, C. Lin, Y. Ren, A. H. MacDonald, and Q. Niu, *Phys. Rev. Lett.* **112**, 206601 (2014).
- [26] J. Li, R.-X. Zhang, Z. Yin, J. Zhang, K. Watanabe, T. Taniguchi, C. Liu, and J. Zhu, *Science* **362**, 1149 (2018).
- [27] J. L. Garcia-Pomar, A. Cortijo, and M. Nieto-Vesperinas, *Phys. Rev. Lett.* **100**, 236801 (2008).
- [28] M. Settnes, S. R. Power, M. Brandbyge, and A.-P. Jauho, *Phys. Rev. Lett.* **117**, 276801 (2016).
- [29] S.-g. Cheng, H. Liu, H. Jiang, Q.-F. Sun, and X. C. Xie, *Phys. Rev. Lett.* **121**, 156801 (2018).
- [30] A. S. Rodin, L. C. Gomes, A. Carvalho, and A. H. Castro Neto, *Phys. Rev. B* **93**, 045431 (2016).
- [31] P. Z. Hanakata, A. Carvalho, D. K. Campbell, and H. S. Park, *Phys. Rev. B* **94**, 035304 (2016).
- [32] C. Chen, X. Chen, Y. Shao, B. Deng, Q. Guo, C. Ma, and F. Xia, *ACS Photonics* **5**, 3814 (2018).
- [33] D. Xiao, M.-C. Chang, and Q. Niu, *Rev. Mod. Phys.* **82**, 1959 (2010).
- [34] Q. Niu, M.-C. Chang, B. Wu, D. Xiao, and R. Cheng, *Physical Effects of Geometric Phases* (World Scientific, Singapore, 2017).
- [35] Y. Li, J. Ludwig, T. Low, A. Chernikov, X. Cui, G. Arefe, Y. D. Kim, A. M. van der Zande, A. Rigosi, H. M. Hill, S. H. Kim, J. Hone, Z. Li, D. Smirnov, and T. F. Heinz, *Phys. Rev. Lett.* **113**, 266804 (2014).

- [36] G. Aivazian, Z. Gong, A. M. Jones, R.-L. Chu, J. Yan, D. G. Mandrus, C. Zhang, D. Cobden, W. Yao, and X. Xu, *Nat. Phys.* **11**, 148 (2015).
- [37] A. Srivastava, M. Sidler, A. V. Allain, D. S. Lembke, A. Kis, and A. Imamoglu, *Nat. Phys.* **11**, 141 (2015).
- [38] D. MacNeill, C. Heikes, K. F. Mak, Z. Anderson, A. Kormányos, V. Zolyomi, J. Park, and D. C. Ralph, *Phys. Rev. Lett.* **114**, 037401 (2015).
- [39] J. Qi, X. Li, Q. Niu, and J. Feng, *Phys. Rev. B* **92**, 121403 (R) (2015).
- [40] C. Jiang, F. Liu, J. Cuadra, Z. Huang, K. Li, A. Rasmata, A. Srivastava, Z. Liu, and W.-B. Gao, *Nat. Commun.* **8**, 802 (2017).
- [41] K. F. Mak, K. He, J. Shan, and T. F. Heinz, *Nat. Nanotechnol.* **7**, 494 (2012).
- [42] H. Zeng, J. Dai, W. Yao, D. Xiao, and X. Cui, *Nat. Nanotechnol.* **7**, 490 (2012).
- [43] T. Cao, G. Wang, W. Han, H. Ye, C. Zhu, J. Shi, Q. Niu, P. Tan, E. Wang, B. Liu, and J. Feng, *Nat. Commun.* **3**, 887 (2012).
- [44] W.-T. Hsu, Y.-L. Chen, C.-H. Chen, P.-S. Liu, T.-H. Hou, L.-J. Li, and W.-H. Chang, *Nat. Commun.* **6**, 8963 (2015).
- [45] K. F. Mak, D. Xiao, and J. Shan, *Nat. Photonics* **12**, 451 (2018).
- [46] Y. Ye, J. Xiao, H. Wang, Z. Ye, H. Zhu, M. Zhao, Y. Wang, J. Zhao, X. Yin, and X. Zhang, *Nat. Nanotechnol.* **11**, 598 (2016).
- [47] K. F. Mak, K. L. McGill, J. Park, and P. L. McEuen, *Science* **344**, 1489 (2014).
- [48] Y. Shimazaki, M. Yamamoto, I. V. Borzenets, K. Watanabe, T. Taniguchi, and S. Tarucha, *Nat. Phys.* **11**, 1032 (2015).
- [49] J. Lee, K. F. Mak, and J. Shan, *Nat. Nanotechnol.* **11**, 421 (2016).
- [50] A. A. High, E. E. Novitskaya, L. V. Butov, M. Hanson, and A. C. Gossard, *Science* **321**, 229 (2008).
- [51] L. Butov, C. Lai, A. Ivanov, A. Gossard, and D. Chemla, *Nature (London)* **417**, 47 (2002).
- [52] E. Hitzer and D. Ichikawa, *Advances in Applied Clifford Algebras* **23**, 887 (2013).
- [53] S. Guan, Y. Liu, Z.-M. Yu, S.-S. Wang, Y. Yao, and S. A. Yang, *Phys. Rev. Mater.* **1**, 054003 (2017).
- [54] Q. Xu, Z. Song, S. Nie, H. Weng, Z. Fang, and X. Dai, *Phys. Rev. B* **92**, 205310 (2015).
- [55] See the Supplemental Material at <http://link.aps.org/supplemental/10.1103/PhysRevLett.124.037701> for details of the first-principles calculation and derivation of the effective model, which includes Refs. [56–61].
- [56] P. E. Blöchl, *Phys. Rev. B* **50**, 17953 (1994).
- [57] G. Kresse and J. Hafner, *Phys. Rev. B* **47**, 558 (1993).
- [58] G. Kresse and J. Furthmüller, *Phys. Rev. B* **54**, 11169 (1996).
- [59] J. P. Perdew, K. Burke, and M. Ernzerhof, *Phys. Rev. Lett.* **77**, 3865 (1996).
- [60] J. Heyd, G. E. Scuseria, and M. Ernzerhof, *J. Chem. Phys.* **118**, 8207 (2003).
- [61] A. Togo, F. Oba, and I. Tanaka, *Phys. Rev. B* **78**, 134106 (2008).
- [62] Y. Zhang, T.-T. Tang, C. Girit, Z. Hao, M. C. Martin, A. Zettl, M. F. Crommie, Y. R. Shen, and F. Wang, *Nature (London)* **459**, 820 (2009).
- [63] A. M. Jones, H. Yu, J. S. Ross, P. Klement, N. J. Ghimire, J. Yan, D. G. Mandrus, W. Yao, and X. Xu, *Nat. Phys.* **10**, 130 (2014).
- [64] Z. Wang, Y.-H. Chiu, K. Honz, K. F. Mak, and J. Shan, *Nano Lett.* **18**, 137 (2018).
- [65] P. Rivera, J. R. Schaibley, A. M. Jones, J. S. Ross, S. Wu, G. Aivazian, P. Klement, K. Seyler, G. Clark, N. J. Ghimire *et al.*, *Nat. Commun.* **6**, 6242 (2015).
- [66] P. Rivera, K. L. Seyler, H. Yu, J. R. Schaibley, J. Yan, D. G. Mandrus, W. Yao, and X. Xu, *Science* **351**, 688 (2016).
- [67] J. S. Ross, P. Rivera, J. Schaibley, E. Lee-Wong, H. Yu, T. Taniguchi, K. Watanabe, J. Yan, D. Mandrus, D. Cobden *et al.*, *Nano Lett.* **17**, 638 (2017).
- [68] P. Rivera, H. Yu, K. L. Seyler, N. P. Wilson, W. Yao, and X. Xu, *Nat. Nanotechnol.* **13**, 1004 (2018).
- [69] C. Jin, E. Y. Ma, O. Karni, E. C. Regan, F. Wang, and T. F. Heinz, *Nat. Nanotechnol.* **13**, 994 (2018).
- [70] H. Yu, Y. Wang, Q. Tong, X. Xu, and W. Yao, *Phys. Rev. Lett.* **115**, 187002 (2015).
- [71] M. Onga, Y. Zhang, T. Ideue, and Y. Iwasa, *Nat. Mater.* **16**, 1193 (2017).
- [72] J. Eisenstein and A. MacDonald, *Nature (London)* **432**, 691 (2004).
- [73] A. A. High, J. R. Leonard, A. T. Hammack, M. M. Fogler, L. V. Butov, A. V. Kavokin, K. L. Campman, and A. C. Gossard, *Nature (London)* **483**, 584 (2012).